Virtual Screening of the Indonesian Medicinal Plant and Zinc Databases for Potential Inhibitors of the RNA-Dependent RNA Polymerase (RdRp) of 2019 Novel Coronavirus

Muhammad Arba[1,*], Andry Nur-Hidayat[1], Ida Usman[2], Arry Yanuar[3], Setyanto Tri Wahyudi[4], Gilbert Fleischer[5], Dylan James Brunt[5], and Chun Wu[5,]**

[1]*Faculty of Pharmacy, Universitas Halu Oleo, Kendari 93232, Indonesia*

[2]*Department of Physics, Universitas Halu Oleo, Kendari 93232, Indonesia*

[3]*Faculty of Pharmacy, Universitas Indonesia, Depok 16424, Indonesia*

[4]*Department of Physics, IPB University, Bogor 16680, Indonesia*

[5]*Department of Molecular & Cellular Biosciences, College of Science and Mathematics, Rowan University, Glassboro, New Jersey 08028, United States*

* ***Corresponding author:***

email: muh.arba@uho.ac.id; wuc@rowan.edu***

Received: May 16, 2020
Accepted: August 3, 2020

DOI: 10.22146/ijc.56120

Abstract: *The novel coronavirus disease 19 (Covid-19) which is caused by severe acute respiratory syndrome coronavirus 2 (SARS-CoV-2) has been a pandemic across the world, which necessitate the need for the antiviral drug discovery. One of the potential protein targets for coronavirus treatment is RNA-dependent RNA polymerase. It is the key enzyme in the viral replication machinery, and it does not exist in human beings, therefore its targeting has been considered as a strategic approach. Here we describe the identification of potential hits from Indonesian Herbal and ZINC databases. The pharmacophore modeling was employed followed by molecular docking and dynamics simulation for 40 ns. 151 and 14480 hit molecules were retrieved from Indonesian herbal and ZINC databases, respectively. Three hits that were selected based on the structural analysis were stable during 40 ns, while binding energy prediction further implied that ZINC1529045114, ZINC169730811, and 9-Ribosyl-trans-zeatin had tighter binding affinities compared to Remdesivir. The ZINC169730811 had the strongest affinity toward RdRp compared to the other two hits including Remdesivir and its binding was corroborated by electrostatic, van der Waals, and nonpolar contribution for solvation energies. The present study offers three hits showing tighter binding to RdRp based on MM-PBSA binding energy prediction for further experimental verification.*

Keywords: *Covid-19; herbal; ZINC; RdRp,* in silico*; coronavirus*

■ INTRODUCTION

The novel coronavirus disease in 2019 (Covid-19) which is caused by severe acute respiratory syndrome coronavirus 2 (SARS-CoV-2) has been declared as a pandemic across the world as it impacts all countries worldwide with more than two million people infected and hundred thousand fatalities [1]. The current situation still has the potential to elevate considering its rapid contagious nature and no drug or vaccine for this particular coronavirus has been found until recently. This necessitates the urgent effort to find small molecules with the potential to inhibit specific proteins of the coronavirus.

Antiviral drug discovery including the 2019 novel coronavirus is subjected to the specific proteins responsible for the viral life cycle continuation. One of the druggable proteins with the potential to target is RNA-dependent RNA polymerase (RdRp) which belongs to the nucleic acid polymerase. The crucial function of RdRp is its role in catalyzing the synthesis of the viral

RNA which is required for viral replication [2-3]. The protein exists in the virus and fortunately not in the host (human body). Therefore, targeting RdRp is considered to have a high potential to inhibit the coronavirus life cycle.

Several small molecules that target RdRp have been reported such as Remdesivir and Sofosbuvir. Remdesivir is a nucleoside analog prodrug and it is reportedly to inhibit SARS-CoV and MERS-CoV [4-5]. Sofosbuvir, on the other side, is a nucleotide analog prodrug, which targets the hepatitis C virus (HCV) infection through HCV NS5B RdRp [6-7]. As it is known that the 2019 nCov-2 coronavirus is a single-strand RNA virus that shares structural similarity with RdRp of Hepatitis-C-Virus (HCV), Ebola, dengue virus, and rhinoviruses, those drugs were also projected for the treatment of the 2019 nCoV-2. However, since the coronavirus is well known for its highly adaptive capability for modified nucleotide analog, the need for novel prompt SARS-CoV-2 antiviral drug discovery was inevitable. Here we performed *in silico* screening based on the pharmacophore features of Remdesivir to find potential compounds for inhibiting RdRp protein. The obtained hits were subjected to molecular docking and molecular dynamics simulation confirmation. We identified several hits molecules with better affinities than Remdesivir according to Molecular Mechanics-Poisson Boltzmann Surface Area (MM-PBSA) protocol.

■ COMPUTATIONAL METHODS

Pharmacophore modeling was performed with the aid of LigandScout 4.3 [8] and the Pharmit web server [9]. In both applications, the structure of Remdesivir (RDM) was used to model pharmacophore. Several pharmacophore features were selected based on the RDM structure and its interaction with the RdRp 2019 nCov2. The 'Max hits per conf' was set to 1 in case of using the Pharmit web server. The selected features were used for screening against the Indonesian Herbal Database (http://herbaldb.farmasi.ui.ac.id/) [10-11] and ZINC [12] databases and the retrieved molecules were submitted for molecular docking. The iDock [13] software was employed for the docking study. The iDock essentially uses the AutoDock Vina machine while adding some features which enable automatic docking of a large compound library. The PDB structure of the RdRp of 2019 novel coronavirus was retrieved from the RCSB protein database using PDB ID 6M71 [14]. Protein structure preparation including adding polar hydrogen atoms and assigning Kollman charges was carried out by using the AutoDock tool (ADT) and the structure was saved in PDBQT format. The grid box for the docking study was defined by following the study of Gao et al. (2020) [14] who indicated the interaction of RDM with the 2019 coronavirus RdRP structure with a grid box size of (x = 40, y = 40, z = 40) and center of (x = 116.02, y = 118.37, z = 127.80) was set which encompass the Remdesivir (RDM) binding site. All ligands were converted to PDBQT format using Open Babel version 2.4.1. Docking analysis was conducted with the Discovery Studio Visualizer 2016.

Prediction of ADME (Absorption, Distribution, Metabolism, Excretion) properties for the two best compounds from ZINC and one compound from HerbalDB databases was performed by using the SwissADME web server (http://www.swissadme.ch) which is developed by the Swiss Institute of Bioinformatics [15]. Each SMILE file of the compound was submitted to the webserver to generate the ADME properties.

The top docked molecules in complex with RdRp and native RdRp were subjected to molecular dynamics (MD) simulation for 40 ns using Amber16 with a time step of 2 fs, periodic boundary conditions, Lennard-Jones (LJ) cutoff of 0.9 nm, and the particle mesh Ewald by following our previous procedure [16]. The ff14SB [17] and GAFF2 [18] were used to assign protein and ligand, respectively. Neutralization was done by introducing sodium ions, while solvation was conducted using the TIP3P water model. Energy minimization was carried out in three steps. The first minimization was carried out using 6000 steps consisting of 500 steepest descent and 5500 steps of the conjugate gradient with protein restrained. Second and third minimization was done using the same steps as the first minimization with the main atoms of protein restrained and without restraint, respectively. After minimization, the system was heated

to 300 K in 150 ps, which was followed by 200 ps equilibration. The final production step was done for 40 ns in the NPT ensemble using pmemd.cuda module of Amber16. Root Mean Square Deviation (RMSD), Root Mean Square Fluctuation (RMSF), hydrogen bond analysis was done using the cpptraj module [19] of Amber16. Also, we performed cluster analysis based on the DBScan algorithm to evaluate the consistency of the initial conformation during the 40 ns MD simulation using the cpptraj module. We used 15 *minpoints* as a threshold to form a cluster with *epsilon* 2.5 Å as distance cutoff for forming a cluster. The PDB structure with the highest chance of occurrence was extracted and employed it as the conformation during 40 ns MD simulation. Finally, the MD trajectory was employed for binding free energy calculation during 40 ns using Molecular Mechanics-Poisson Boltzmann solvent accessible surface area (MM-PBSA) method [19-21] as implemented in MMPBSA.py module of Amber16 software. Considering the highly charged binding interface of ligand-RdRp complex, we employed the solute dielectric constant 4 in the MM-PBSA binding energy calculation.

■ RESULTS AND DISCUSSION

The study was initiated with the analysis of the structure of Remdesivir (RDM). It is known that RDM is a prodrug and when binding to RdRp, it is converted to its tri-phosphate form. Therefore, the active form of RDM was used for further analysis. Fig. 1 displays the structure of RDM and its active form.

The pharmacophore features of RDM consisted of one aromatic ring, five hydrogen bond donor, sixteen hydrogen bond acceptor, three negative ions (phosphate atoms), and one hydrophobic feature. However, only five features were selected in LigandScout 4.3 to increase the potential hit molecules gain, which includes one aromatic, one hydrogen bond donor, and three hydrogen bond acceptors. Screening against the Indonesian Herbal database resulted in 151 hit molecules gain. The same features were employed when screening using the Pharmit web server, in which screening against the ZINC database retrieved 14480 hit molecules. Fig. 2 displays the selected features of pharmacophore in the LigandScout 4.3 and Pharmit web server.

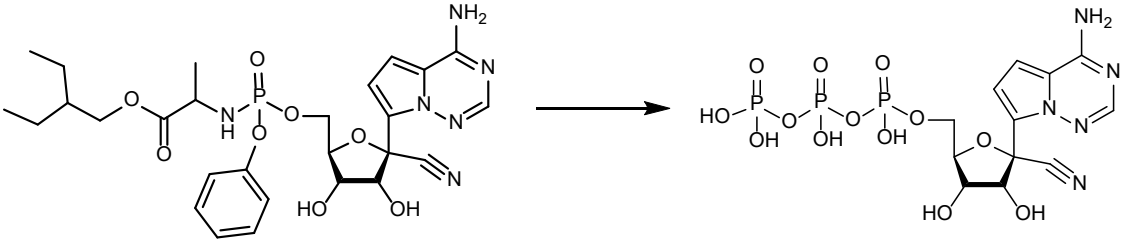

Fig 1. The 2D structures of Remdesivir (left) and its active form (right)

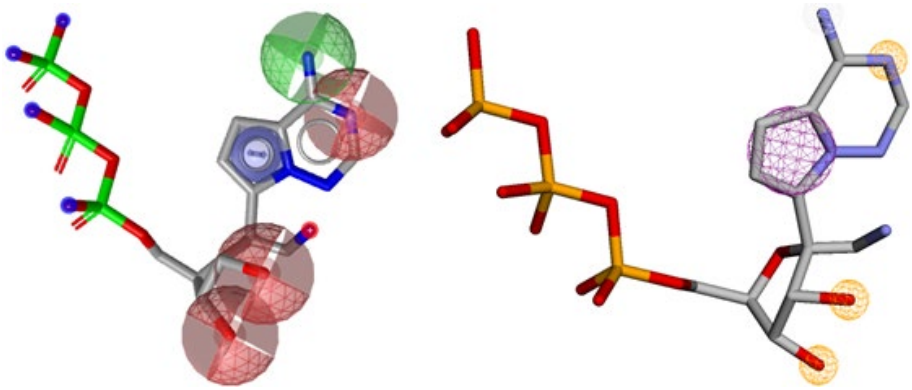

Fig 2. The pharmacophore features selected for screening with one aromatic (blue and purple circles), one hydrogen bond donor (green and white circles), and three hydrogen bond acceptors (red and yellow circles) features employed for screening in LigandScout and Pharmit web server, respectively

Molecular docking of 14480 hits molecules and 151 molecules retrieved from ZINC and Indonesian Herbal databases, respectively, was performed in the putative of the binding site of RDM. It is known that the structure of RNA-dependent RNA polymerase of SARS-CoV-2 form "right hand" conformation and contains three domains, which is similar to the structure of SARS coronavirus (SARS-CoV) [14,20-21]. A finger subdomain spans from Ser397 to Ala581 and Lys621 to Gly679, a palm subdomain is located at Thr582 to Pro620 and Thr680 to Gln815, while the thumb subdomain was positioned at His816 to Glu920. The active site of the 2019 SARS-CoV-2 is located in the palm domain which consisted of motif A, B, C, D, E, F, and G. The binding model of RDM to the RdRp is supposedly surrounded by Asp618, Asp623 (motif A), Thr680, Ser682, Asn691 (motif B), Ser759, Asp760, and Asp761 (motif C) [14]. The binding site of RDM is depicted in Fig. 3. This site was also identified as the top 1 site by the SiteMap module of the Schrodinger Package (Release 2019-4).

The docking of RDM at the supposed binding site gave the binding energy of −6.96 kcal/mol, while docking of 14480 hit molecules yielded binding energies from −4.42 kcal/mol to −12.36 kcal/mol. On the other hand, docking 151 molecules gave binding energies between −5.2 and −10.65 kcal/mol. All docking results were analyzed for their ligand structures and interactions with RdRp and based on the structural comparison between hit molecules and Remdesivir for mimicking nucleotide structure, we selected one compound from the Indonesian Herbal Database and two compounds from the ZINC database for subjecting to 40 ns MD simulation. Fig. 4 displays the two-dimensional best docked hit molecules.

The best docked hit molecules show a similar interaction with Remdesivir (RDM). Table 1 tabulates the binding energy and interactions with RdRp.

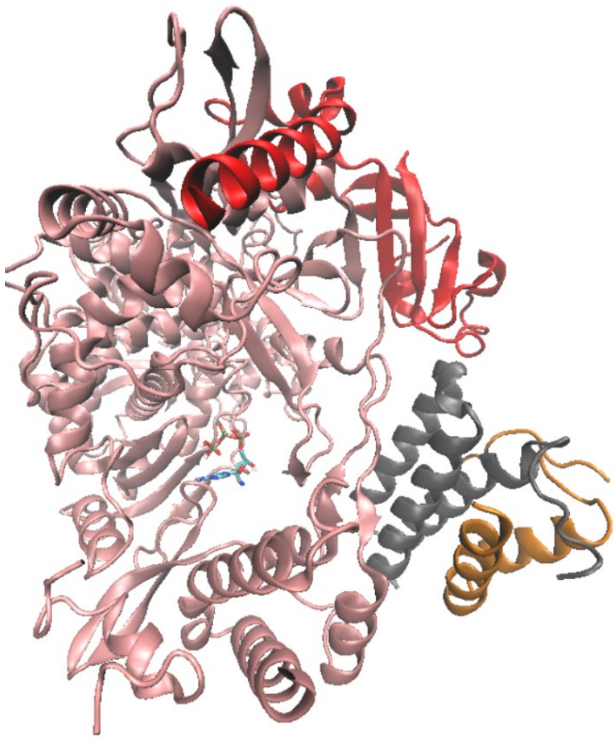

Fig 3. The putative ligand-binding site of RDM to RdRp, in which carbon and oxygen atoms of active RDM were colored blue and red, respectively

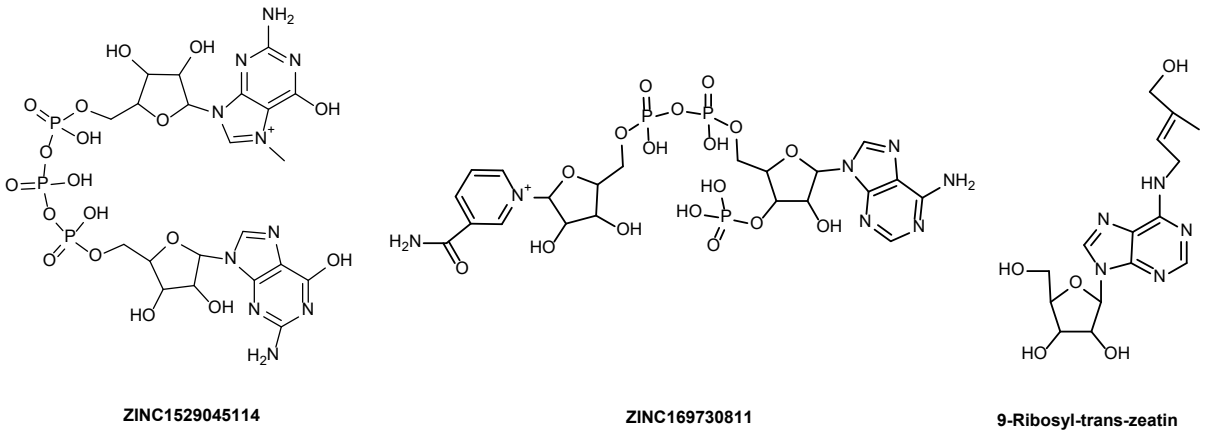

Fig 4. The two-dimensional best docked hit molecules

Table 1. The binding affinities and interactions between hit molecules and RdRp

Ligand	Binding affinities (kcal/mol)	H-bond (distance, Å)	Electrostatic interactions	Hydrophobic
RDM	−6.96	Tyr619 (3.22) Ser814 (3.12) Asp760 (2.32) Asp761 (2.21) Glu811 (3.36) Lys798 (2.72)	Asp618 Asp760 Asp761 Glu811	
ZINC1529045114	−8.07	Lys621 (2.87) Arg624 (3.06) Thr687 (2.69) Asn691 (3.26) Asp452 (3.37) Asp623 (3.04)	Asp623 Asp760	Arg555
ZINC169730811	−8.04	Tyr619 (3.32) Cys622 (3.10) Glu811 (3.26)	Arg624 Asp623	Lys798
9-Ribosyl-trans-zeatin	−10.65	Asp761 (2.34) Glu811 (2.43) Tyr619 (2.64) Asp760 (2.84)		Cys622

Interaction of ZINC1529045114 was supported by hydrogen bonds between the oxygen atom of the phosphate group with Lys621, as well as the nucleoside group with Thr687, Asn691, Asp452, Asp623, and Arg624. The purine group also contributed to the electrostatic interactions through pi-anion interactions with Asp623 and Asp760. In the meantime, the interaction of ZINC169730811 was based on the hydrogen bond interactions with Tyr619 through the oxygen atom of the phosphate group, as well as with Cys622 through the oxygen of the oxolane group. The hydrogen bond interaction was also observed with Glu811, while electrostatic interactions between pi-electron of purine group and Arg624 and Asp623 were observed. Also, hydrophobic interaction with Lys798 was noted. While hydrogen bonding interactions for 9-Ribosyl-trans-zeatin occurred with Asp761, Glu811, Tyr619, and Asp760. In the meanwhile, Remdesivir (RDM) showed hydrogen bonding interactions with Tyr619, Ser814, Asp760, Asp761, Glu811, and Lys798. Electrostatic interactions with Asp618, Asp760, Asp761, and Glu811 were observed between RDM and RdRp. Fig. 5 displays the interaction of each hit molecule with the RdRp.

Prediction of ADME Properties

Table 2 shows the predicted ADME properties for the three compounds. The ZINC1529045114, ZINC169730811, and 9-Ribosyl-trans-zeatin show low intestinal absorption properties with no chance for distribution into the brain. The three compounds also could not be inhibitors for the subtypes of cytochrome P450 enzymes (CYPs) including CYP1A2, CYP2C19, CYP2C9, CYP2D6, and CYP3A4, which indicated that the two compounds could not probably be metabolized. Compound 9-Ribosyl-trans-zeatin fulfill the conditions of drug-likeness properties without any violation of Lipinski rule of five including MV < 500, calculated octanol-water partition coefficient (LogP) ≤ 5, some hydrogen bonding acceptors ≤ 10, as well as several hydrogen bonding donors ≤ 5. All the three compounds have a minor *in silico* ADME properties for oral administration, which indicated their favorable use in prodrug form.

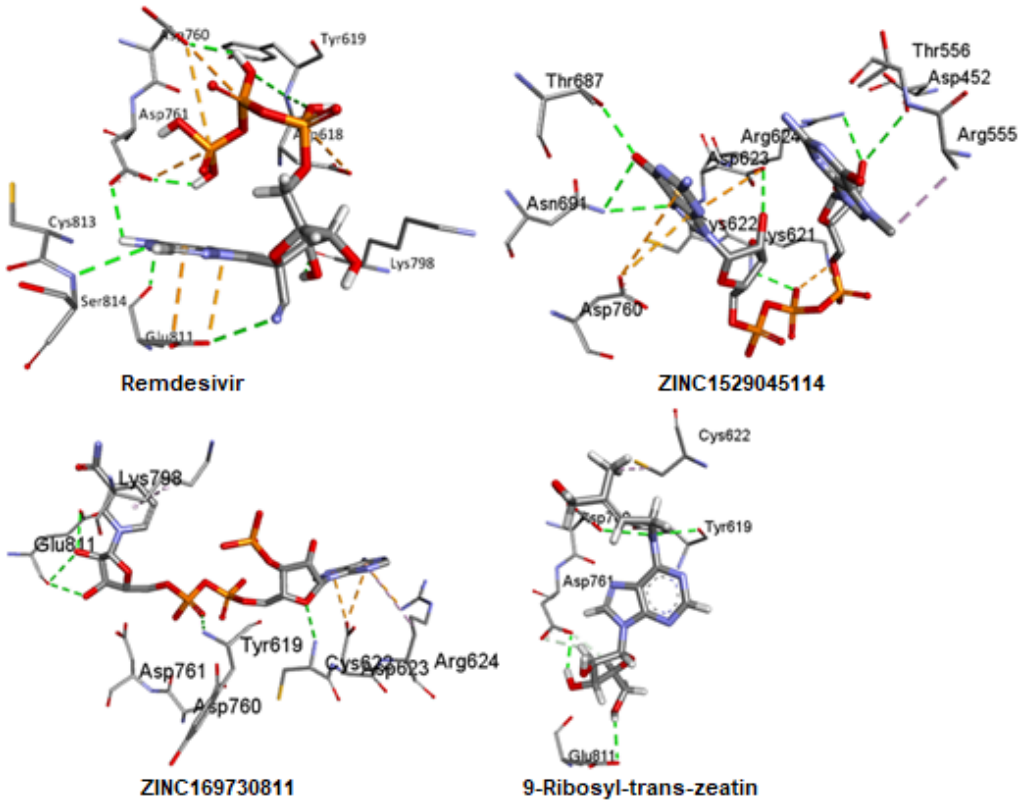

Fig 5. The interaction of each hit molecules with RdRp. The green, orange, and purple dashed lines represent hydrogen bond, electrostatics, and hydrophobic interactions, respectively

Table 2. The predicted ADME properties

Compound	GI absorption	BBB permeant	CYP1A2	CYP2C19	CYP2C9	CYP2D6	CYP3A4	Lipinksi rule
RDM	Low	No	No	No	No	No	No	3 violations (MW>500, N or O>10, NH or OH>5)
ZINC1529045114	Low	No	No	No	No	No	No	3 violations (MW>500, N or O>10, NH or OH>5)
ZINC169730811	Low	No	No	No	No	No	No	2 violations (MW>500, N or O>10)
9-Ribosyl-trans-zeatin	Low	No	No	No	No	No	No	0 violation

Molecular dynamics simulation was performed to analyze the impact of ligand binding to the RdRp stability, which was estimated using the RMSD values of the receptor backbone atoms. Fig. 6 displays the RMSD values for receptor backbone atoms of each complex and native apo RdRp (without ligand) as a function of 40 ns simulation time. It is noted that the native apo RdRp and protein-ligand complexes reached equilibrium during the 40 simulations. The RMSD values of 9-Ribosyl-trans-zeatin were higher than those of other compounds. ZINC1529045114, ZINC169730811, and RDM display fluctuation in the early 20 ns especially for RDM and ZINC169730811. However, those three complexes become stable after around 25 ns and the curve fluctuation of ZINC169730811 was lower than those two ligands, which implied that ZINC169730811 could form a more stable complex with RdRp.

On the other hand, residue fluctuation during ligand binding was recorded as RMSF values of the native apo RdRp and four complexes as shown in Fig. 7.

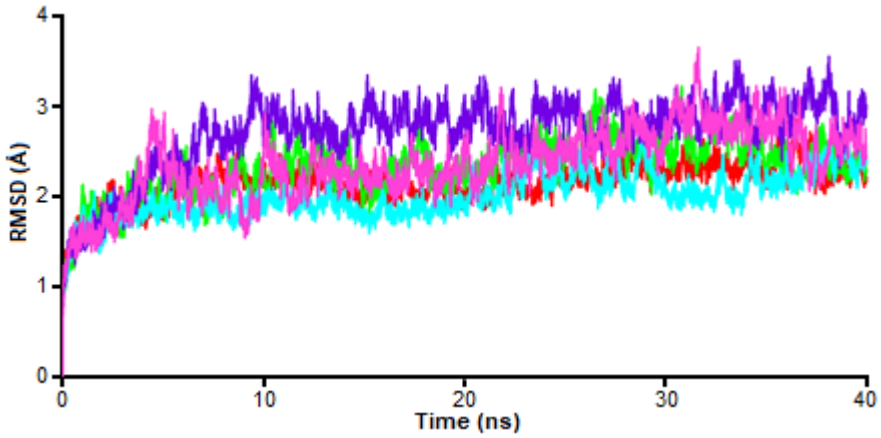

Fig 6. The RMSD values for the receptor backbone atoms of each complex of RDM (red), ZINC1529045114 (green), ZINC169730811 (blue), 9-Ribosyl-trans-zeatin (purple), and native apo RdRp (pink)

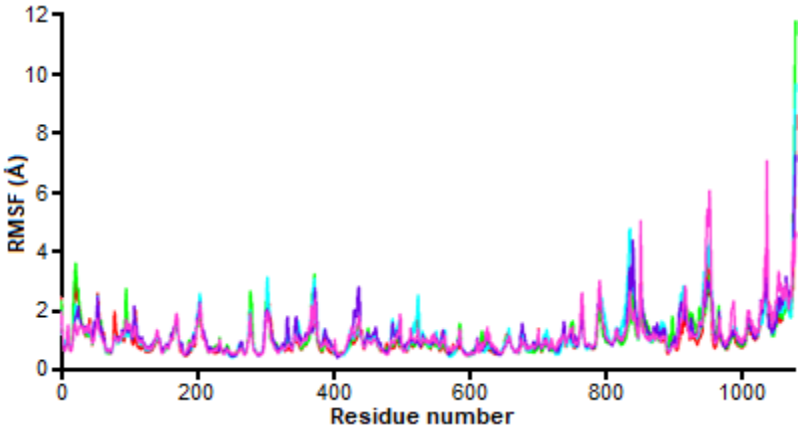

Fig 7. A plot of residue fluctuation during ligand binding was recorded as RMSF values as RDM (red), ZINC1529045114 (green), ZINC169730811 (blue), 9-Ribosyl-trans-zeatin (purple), and receptor only (pink)

The RMSF values indicated that the higher RMSF values, the more fluctuation amino acid residues during MD simulation. As shown in Fig. 7, the highest peak was located at residue 1078 which was corresponded to the amino-terminal region of the protein, which is typical in all protein fluctuation. Peaks around 810 and 980, 300, 380, and 20 have more fluctuated around 4 Å than other regions, which is attributable to residues in tails. The amino acids involved in the ligand-binding including Tyr560 (Tyr619), Lys562 (Lys621), Cys563 (Cys622), Asp564 (Asp623), Arg565 (Arg624), Thr628 (Thr687), Asn632 (Asn691), Asp701 (Asp760), Asp702 (Asp761), Glu752 (Glu811) as well as the rest of residues was stable enough under 3 Å and each ligand-induced the similar pattern of RMSF fluctuation.

Trajectory clustering was employed to identify the most populated structure for each complex. It is found out that the percentage of clusters was 100% in each complex (Table S2). Fig. 8 displays the single-populated structure of each ligand and their superimposition, while Fig. 9 depicts their detailed interactions. The single populated structure of RDM resulted in tight interactions with key residues of RdRp such as Asp701 (Asp760) and Asp559 (Asp618). The most abundant structure of ZINC1529045114 was also involving key residues of RdRp such as Asp564 (Asp623), Asp701 (Asp760), and Thr621 (Thr680). Similar interactions were also observed in the most abundant structure of ZINC169730811 which include Arg496 (Arg555), Asp564 (Asp623), and Asp702 (Asp761). While the most abundant of the 9-Ribosyl-trans-zeatin structure includes interactions with Asp564 (Asp623), Asp559

(Asp618), and Arg496 (Arg555). As Zhao et al. (2020) [14] reported the key residues of Asp618, Asp623, Asp760, Asp761, Thr680, Arg555, and Asn691, was supposed to interact with Remdesivir (RDM).

Additionally, the hydrogen bond occupancies were also monitored during the trajectory period of the MD run. Table S1 shows the hydrogen bonding profile for each complex. The complex of ZINC169730811 showed hydrogen bonding higher occupancies than that of ZINC1529045114 and 9-Ribosyl-trans-zeatin. The highest occupancy was observed between ZINC169730811 and Asp702 (Asp761) with 80.78%, followed by moderate occupancies with Lys492 (Lys551) (32.53%). While the highest hydrogen bonding occupancy occurring in ZINC1529045114 was detected with Arg496 (Arg555) (45.55%), followed by hydrogen bonding moderate occupancy with Arg565 (Arg624) (30.18%) and Asp701 (Asp760) (29.6%) and Asp564 (Asp623) (28.95%). While those observed in 9-Ribosyl-trans-zeatin occurred with low occupancies, for example, occupancies of hydrogen bonding with Glu752 (Glu811) and Asp702 (Asp761) were 37.66% and 23.14%, respectively. From the data shown, it can be concluded that ZINC169730811 has better binding stability than ZINC1529045114 and 9-Ribosyl-trans-zeatin.

Binding Free Energy Calculation

The enthalpy terms of binding affinities of hit molecules were calculated using MM-PBSA methods as reflected in Table 3, while due to complexity, the entropy part was not calculated. The MM-PBSA binding energy offers a good compromise between accuracy and computational cost [22-25].

The ZINC169730811 displays the lowest total interaction energies (ΔE_{PBTOT} = −57.73±4.49 kcal/mol), followed by ZINC1529045114 (−30.29±4.38 kcal/mol), 9-Ribosyl-trans-zeatin (−20.79±4.19 kcal/mol) and RDM (−17.87±4.19 kcal/mol). The electrostatic energy value (ΔE_{ELE} = −45.31±7.30 kcal/mol) was favorable for the binding of ZINC169730811 as in the case of ZINC1529045114 (ΔE_{ELE} = −46.46±7.84 kcal/mol), RDM (−39.29±4.78 kcal/mol), and 9-Ribosyl-trans-zeatin (−14.06±4.60 kcal/mol). The favorable energy terms were also contributed by the lower van der Waals energy (ΔE_{VDW} = −58.77±4.29 kcal/mol), ZINC1529045114 (ΔE_{VDW} = −37.05±4.49 kcal/mol), 9-Ribosyl-trans-zeatin (ΔE_{VDW} = −21.75±5.57 kcal/mol) and RDM (ΔE_{VDW} = −15.72±5.29 kcal/mol). The binding of ligands was also corroborated by lower nonpolar contribution for solvation energy (ΔE_{PBSUR} = −6.22±0.26 kcal/mol), −4.56±0.20 kcal/mol, −3.56±0.32 kcal/mol, and −3.34±0.31 kcal/mol for ZINC169730811, ZINC1529045114, RDM, and 9-Ribosyl-trans-zeatin, respectively. The superiority of the binding energy of ZINC169730811 to other ligands was also reflected in Fig. S1 which shows the plot of MM-PBSA binding energy

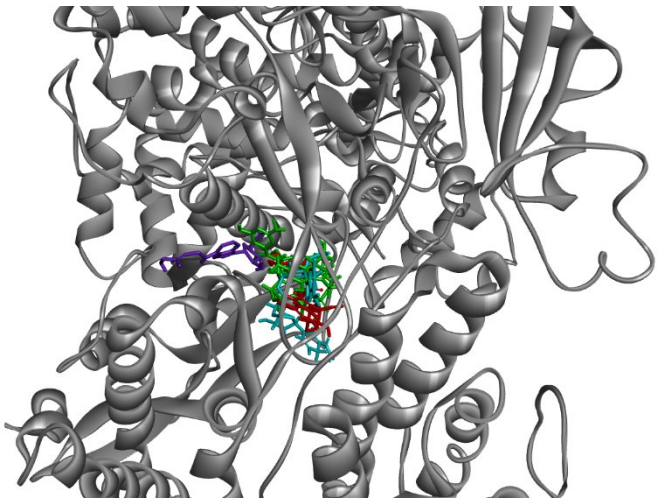

Fig 8. The superimposition of single populated structures in which RDM, ZINC1529045114, ZINC169730811, and 9-Ribosyl-trans-zeatin are colored as red, green, blue, and purple, respectively

Table 3. The binding energy for the last 10 ns predicted by MM-PBSA protocol.

Ligand	ΔE_{ELE} (kcal/mol)	ΔE_{VDW} (kcal/mol)	ΔE_{PB} (kcal/mol)	ΔE_{PBSUR} (kcal/mol)	ΔE_{PBTOT} (kcal/mol)
ZINC1529045114	−46.46±7.84	−37.05±4.49	57.78±6.42	−4.56±0.20	−30.29±4.38
ZINC169730811	−45.31±7.30	−58.77±4.29	52.58±5.36	−6.22±0.26	−57.73±4.49
9-Ribosyl-trans-zeatin	−14.06±4.60	−21.75±5.57	18.36±3.19	−3.34±0.31	−20.79±4.19
RDM	−39.29±4.78	−15.72±5.29	40.71±4.02	−3.56±0.32	−17.87±4.19

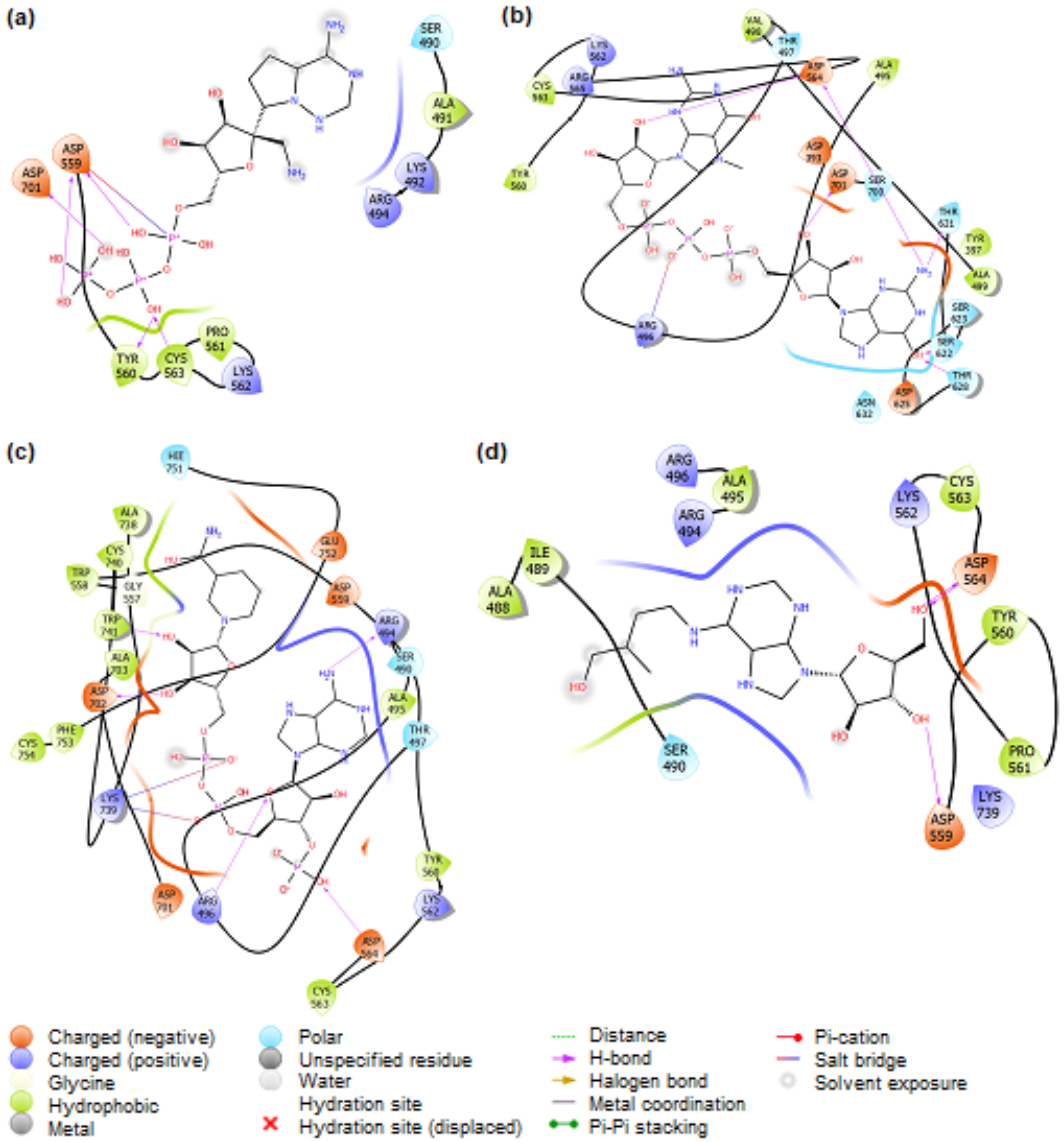

Fig 9. The single populated pose of each ligand. (a) RDM (b) ZINC1529045114 (c) ZINC169730811 (d) 9-Ribosyl-trans-zeatin

throughout simulation time, in which ZINC169730811 has the lowest binding energy in the whole simulation time. It is worth to note that the three-hit molecules display lower binding energies than that of RDM, which is indicated their tighter affinities toward the RdRp protein.

■ CONCLUSION

In brief, the present study employed pharmacophore modeling for identifying hit molecules from both Indonesian herbal and ZINC databases potential for binding to RNA-dependent RNA polymerase (RdRp) of SARS-CoV-2. One hit from herbal and two hits from ZINC databases was selected for MD simulation, and the three hits showing tighter binding to RdRp based on MM-PBSA binding energy prediction. The present study suggests the three hits as potential inhibitors of RdRp, however, further experimental verification is required.

■ ACKNOWLEDGMENTS

This study was supported by the Ministry of Research and Technology/National Board of Research and Innovation, the Republic of Indonesia. C.W. also acknowledges the support from US National Science

Foundation under Grants NSF RUI-1904797 and XSEDE MCB 170088. We acknowledge Prof. Rao for offering us the cryo-EM structure of RdRp (PDB ID: 6M71) before its availability from the Protein Data Bank.

■ AUTHOR CONTRIBUTIONS

MA, AH, and IU design and experimented, AY support the herbal database, GF and DJB wrote the manuscript, CW supervised the experiment. All authors agreed to the final version of this manuscript.

■ REFERENCES

[1] World Health Organization, 2020, *Coronavirus Disease (COVID-2019): Situation Reports, 94*, World Health Organization, Geneva, 12.

[2] Dolan, P.T., Whitfield, Z.J., and Andino, R., 2018, Mechanisms and concepts in RNA virus population dynamics and evolution, *Annu. Rev. Virol.*, 5 (1), 69–92.

[3] Jia, H., and Gong, P., 2019, A structure-function diversity survey of the RNA-dependent RNA polymerases from the positive-strand RNA viruses, *Front. Microbiol.*, 10, 1945.

[4] Agostini, M.L., Andres, E.L., Sims, A.C., Graham, R.L., Sheahan, T.P., Lu, X., Smith, E.C., Case, J.B., Feng, J.Y., Jordan, R., Ray, A.S., Cihlar, T., Siegel, D., Mackman, R.L., Clarke, M.O., Baric, R.S., and Denison, M.R., 2018, Coronavirus susceptibility to the antiviral Remdesivir (GS-5734) is mediated by the viral polymerase and the proofreading exoribonuclease, *MBio*, 9 (2), e00221-18.

[5] Gordon, C.J., Tchesnokov, E.P., Feng, J.Y., Porter, D.P., and Götte, M., 2020, The antiviral compound Remdesivir potently inhibits RNA-dependent RNA polymerase from Middle East respiratory syndrome coronavirus, *J. Biol. Chem.*, 295 (15), 4773–4779.

[6] Götte, M., and Feld, J.J., 2016, Direct-acting antiviral agents for hepatitis C: Structural and mechanistic insights, *Nat. Rev. Gastroenterol. Hepatol.*, 13 (6), 338–351.

[7] Gane, E.J., Stedman, C.A., Hyland, R.H., Ding, X., Svarovskaia, E., Symonds, W.T., Hindes, R.G., and Berrey, M.M., 2013, Nucleotide polymerase inhibitor sofosbuvir plus ribavirin for Hepatitis C, *N. Engl. J. Med.*, 368 (1), 34–44.

[8] Wolber, G., and Langer, T., 2005, LigandScout: 3-D pharmacophores derived from protein-bound ligands and their use as virtual screening filters, *J. Chem. Inf. Model.*, 45 (1), 160–169.

[9] Sunseri, J., and Koes, D.R., 2016, Pharmit: interactive exploration of chemical space, *Nucleic Acids Res.*, 44 (W1), W442–W448.

[10] Yanuar, A., Mun'im, A., Lagho, A.B.A., Syahdi, R.R., Rahmat, M., and Suhartanto, H., 2011, Medicinal plants database and three dimensional structure of the chemical compounds from medicinal plants in Indonesia, *Int. J. Comput. Sci. Issues*, 8 (5), 180–183.

[11] Arba, M., Pangan, A., and Yanuar, A., 2020, The search for peptide deformylase inhibitor from Indonesian medicinal plant database: An *in-silico* investigation, *Biointerface Res. Appl. Chem.*, 10 (2), 5117–5121.

[12] Irwin, J.J., Sterling, T., Mysinger, M.M., Bolstad, E.S., and Coleman, R.G., 2012, ZINC: A free tool to discover chemistry for biology, *J. Chem. Inf. Model.*, 52 (7), 1757–1768.

[13] Li, H., Leung, K.S., and Wong, M.H., 2012, idock: A multithreaded virtual screening tool for flexible ligand docking, *IEEE Symposium on Computational Intelligence in Bioinformatics and Computational Biology (CIBCB)*, San Diego, United States, 9-12 May 2012, 77–84.

[14] Gao, Y., Yan, L., Huang, Y., Liu, F., Zhao, Y., Cao, L., Wang, T., Sun, Q., Ming, Z., Zhang, L., Ge, J., Zheng, L., Zhang, Y., Wang, H., Zhu, Y., Zhu, C., Hu, T., Hua, T., Zhang, B., Yang, X., Li, J., Yang, H., Liu, Z., Xu, W., Guddat, L.W., Wang, Q., Lou, Z., and Rao, Z., 2020, Structure of the RNA-dependent RNA polymerase from COVID-19 virus, *Science*, 368 (6492), 779–782.

[15] Daina, A., Michielin, O., and Zoete, V., 2017, SwissADME: A free web tool to evaluate pharmacokinetics, drug-likeness and medicinal chemistry friendliness of small molecules, *Sci. Rep.*, 7, 42717.

[16] Arba, M., and Nurmawati, O., 2020, Identification of potential inhibitors for Bruton's Tyrosine Kinase (BTK) based on pharmacophore-based virtual screening, *Biointerface Res. Appl. Chem.*, 10 (3), 5472–5477.

[17] Maier, J.A., Martinez, C., Kasavajhala, K., Wickstrom, L., Hauser, K.E., and Simmerling, C., 2015, ff14SB: Improving the accuracy of protein side chain and backbone parameters from ff99SB, *J. Chem. Theory Comput.*, 11 (8), 3696–3713.

[18] Wang, J., Wolf, R.M., Caldwell, J.W., Kollman, P.A., and Case, D.A., 2004, Development and testing of a general amber force field, *J. Comput. Chem.*, 25 (9), 1157–1174.

[19] Roe, D.R., and Cheatham III, T.E., 2013, PTRAJ and CPPTRAJ: Software for processing and analysis of molecular dynamics trajectory data, *J. Chem. Theory Comput.*, 9 (7), 3084–3095.

[20] Appleby, T.C., Perry, J.K., Murakami, E., Barauskas, O., Feng, J., Cho, A., Fox, D., Wetmore, D.R., McGrath, M.E., Ray, A.S., Sofia, M.J., Swaminathan, S., and Edwards, T.E., 2015, Structural basis for RNA replication by the hepatitis C virus polymerase, *Science*, 347 (6223), 771–775.

[21] Deval, J., Symons, J.A., and Beigelman, L., 2014, Inhibition of viral RNA polymerases by nucleoside and nucleotide analogs: Therapeutic applications against positive-strand RNA viruses beyond hepatitis C virus, *Curr. Opin. Virol.*, 9, 1–7.

[22] Rifai, E.A., Ferrario, V., Pleiss, J., and Geerke, D.P., 2020, Combined linear interaction energy and alchemical solvation free-energy approach for protein-binding affinity computation, *J. Chem. Theory. Comput.*, 16 (2), 1300–1310.

[23] Kollman, P.A., Massova, I., Reyes, C., Kuhn, B., Huo, S., Chong, L., Lee, M., Lee, T., Duan, Y., Wang, W., Donini, O., Cieplak, P., Srinivasan, J., Case, D.A., and Cheatham, T.E., 2000, Calculating structures and free energies of complex molecules: Combining molecular mechanics and continuum models, *Acc. Chem. Res.*, 33 (12), 889–897.

[24] Srinivasan, J., Cheatham, T.E., Cieplak, P., Kollman, P.A., and Case, D.A., 1998, Continuum solvent studies of the stability of DNA, RNA, and phosphoramidate–DNA helices, *J. Am. Chem. Soc.*, 120 (37), 9401–9409.

[25] Arba, M., Ruslin, Ihsan, S., Tri Wahyudi, S., and Tjahjono, D.H., 2017, Molecular modeling of cationic porphyrin-anthraquinone hybrids as DNA topoisomerase IIβ inhibitors, *Comput. Biol. Chem.*, 71, 129–135.